Distinction of the irreversible and reversible actuation regions of B-doped poly-Si based electrothermal actuators

S Deladi, G J M Krijnen and M C Elwenspoek

MESA+ Research Institute, University of Twente/Transducers Science and Technology,
PO Box 217, 7500 AE Enschede, The Netherlands

E-mail: s.deladi@ewi.utwente.nl

Abstract

Polycrystalline-Si microactuators based on electrothermal principles exhibit many interesting features but their practical use is severely limited by permanent damage that may occur due to accidental overheating. Under these conditions, polycrystalline-Si structures will display irreversible structural changes ranging from slight geometrical deformations to complete damage. In this paper, an approach is presented to avoid permanent structural deformation of B-doped polycrystalline-Si based electrothermal actuators by overheating. The method allows us to distinguish reversible and irreversible actuation conditions and is demonstrated under environmental and vacuum conditions. It enables full utilization of the capabilities of B-doped polycrystalline-Si based electrothermal actuators with reproducible performance.

1. Introduction

Electrothermal actuators are used for applications requiring large forces and low actuation voltages such as micromotors [1–3], exploiting their main advantages compared to electrostatic actuators. However, very high local temperatures obtained by Joule heating limit the utilization of electrothermal actuators and need to be avoided. At relatively high electrical power, actual values being determined by design and environmental conditions, the actuator changes its neutral position and materials properties, resulting in irreversible change of the geometrical shape. The phenomenon has been reported by different authors, calling it 'plastic deformation' [4] or 'back bending' [1, 2] and it is explained as a result of a reflow or recrystallization of the material at high temperatures [1] or caused by the stress in the hot arm when the temperature rises to above the brittle-to-ductile transition (approximately 660 °C for polycrystalline Si) [4].

To the best of our knowledge the only way to actuate the B-doped Si or polycrystalline-Si based electrothermal actuators with reproducible performance is to operate them below the intrinsic temperature [5]. At this temperature, the intrinsic and dopant carrier concentrations are equal.

The dopant concentration for polycrystalline-Si at which the number of active carriers saturates is approximately 2×10^{20} [6]. According to [7], higher dopant concentration causes higher intrinsic temperature that can be well above the temperature limit at which plastic deformation initiates due to Joule heating.

Our concern about reversible and irreversible actuation regions of electrothermal actuators originates from investigations on a microtribotester that requires large in- and out-of-plane forces for adhesion, friction and wear studies of various material couples [8–10]. Electrothermal actuators have been designed or adopted from the literature to cover the ranges of forces and displacements for this purpose. The structural material of the actuators is polycrystalline-Si (poly-Si) since the electrical properties can be controlled by the amount of B diffused into the poly-Si and because it is suitable for all types of electrothermal actuators whether the working principle is any of the following: (i) the mismatch between thermal expansion of unlike materials (bimorph effect) [11, 12]; (ii) based on the differential expansion of various geometries micromachined from the same material [13–15]; (iii) thermal expansion of constrained structures [9, 16–18].
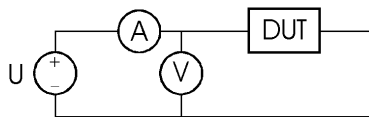
Figure 1. Schematic of the electrical circuit used for device characterization.

The experimental method presented focuses on the onset of the deviation from the neutral position of the B-doped polycrystalline-Si based electrothermal actuators.

2. Distinction of reversible and irreversible actuation regions

In order to distinguish the reversible and irreversible operating regions, experiments have been carried out on electrothermal actuators with the working principle from all three categories mentioned above. The design rules as well as their simulated and experimental performance have been reported earlier [8, 9] where also the importance of taking the temperature dependence of the properties of the materials into account has been shown. The actuators presented are all surface micromachined, only the embedding in complex MEMS devices needs special requirements [10]. They were fabricated in one and the same batch and the thicknesses of the layers are: poly-Si—1.6 μm, Si-rich nitride (SiRN)—0.25 μm, and Si-oxide—0.8 μm (where applicable). The gap between the substrate and the free structures is 2 μm. The measured resistivity of the B-doped poly-Si was 3×10^{-3} Ω cm at room temperature, which corresponds to a doping concentration of approximately 8×10^{19} atoms cm^{-3} [6]. The resistivity of highly doped poly-Si approaches the resistivity of highly doped single-crystal Si [6], thus the estimated intrinsic temperature of the poly-Si with a doping concentration of 8×10^{19} B atoms cm^{-3} [7] is 1300 K.

The actuators were driven by voltage control. The schematic of the electrical circuit used for device characterization is presented in figure 1. Resistance and operational power were calculated from the voltage of the source and the measured current. The serial resistance of the electrical connection was very low compared to the resistance of the actuators, therefore it was neglected in the interpretation of measurements.

A micrometer mounted on an optical microscope was used for the measurement of vertical displacements in ambient conditions, while under vacuum, the measurement of the out-of-plane displacement is based on pictures captured during actuation on the SEM-table tilted relative to the horizontal. In-plane displacements have been measured directly with the optical microscope in ambient condition and based on SEM photographs under vacuum. The measurements are presented for different actuators in ambient conditions or/and under vacuum in order to emphasize that the distinction method of reversible and irreversible actuation regions is applicable for operation in both conditions.

The measurement procedure is the following: I—identification of the initial neutral position of the actuator; II—actuation at a certain electrical power, then measurement of the displacement and electrical resistance after 1 min; III—power switched off and measurement of the neutral
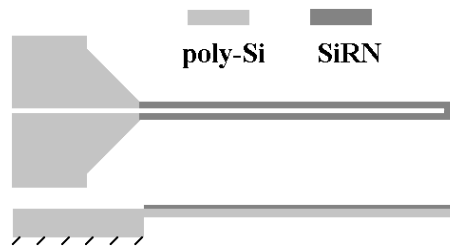
Figure 2. Sketch of the bimorph actuator: top-view (upper graph) and cross-view (lower graph).
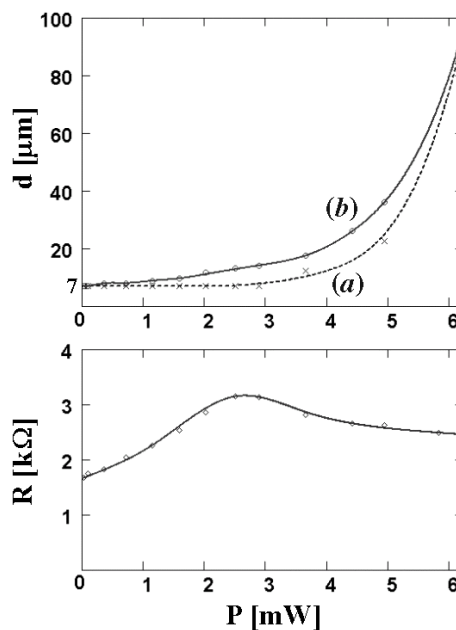
Figure 3. Maximum tip displacement versus electrical power and electrical resistance versus power characteristics of the bimorph actuator (under vacuum): (*a*) neutral position; (*b*) maximum tip deflection.

Table 1. Geometrical characteristics—bimorph actuator.

Geometrical characteristics	Dimensions (μm)
Legs	352×4
Connection of the legs at tip	20×13
Contact pads	100×100

position after 1 min. Subsequently the actuation power is incremented and the measurement cycle is repeated (II and III) till the failure of the actuator occurs. The results are collected in the maximum tip displacement versus electrical power and electrical resistance versus power characteristics for each type of actuator.

2.1. Bi- and trimorph actuators

These actuators belong to the first category (i) and they consist of two or three layers of unlike materials. The sketch and the geometrical characteristics of the bimorph actuator are given in figure 2 and table 1 respectively.

The measurements performed in step III form the curve (*a*) of the displacement versus power characteristic (figure 3), representing the change of the neutral position of the actuator,
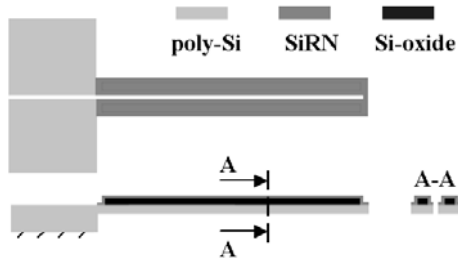
Figure 4. Sketch of the trimorph actuator: top-view (upper graph) and cross-view (lower graph).

Table 2. Geometrical characteristics—trimorph actuator.

Geometrical characteristics	Dimensions (μm)
Legs	330×20
Si-oxide	312×12
Connection of the legs at tip	4×5
Contact pads	118×110

while curve (b) shows the maximum displacement of the tip for the range of actuation powers and it consists of measurement data from step II. Curves are drawn through the measurement points to guide the eye. The effective displacement that the actuator provides for a certain power is the difference between curves (a) and (b). The shift of the initial neutral position of the actuator from the horizontal position '0' after fabrication (figure 3) is caused by the stress gradient across the bimorph structure (SiRN on top of poly-Si). By increasing the actuation power the displacement becomes larger and larger. From measurements performed for a range of actuation powers, it turned out that the actuator could not regain its initial neutral position after a certain threshold value (2.5 mW for the device with geometrical characteristics in table 1) had been exceeded, and by applying higher electrical power the neutral position shifted more and more till the failure of the actuator occurred due to reaching the melting temperature of the poly-Si.

By analyzing the characteristics presented in figure 3 we can observe that the change of the neutral position of the actuator initiates when the value of the electrical resistance during operation of the device reaches a maximum. This is also confirmed by measurements on the trimorph actuator (figure 4, table 2) under vacuum.

In this case the shift of the initial neutral position from the horizontal is negative (figure 5) due to combination of highly compressive Si-oxide, tensile SiRN and almost stress-free B-doped poly-Si. The electrical resistance versus actuation power characteristic shows the same trend as the one of the bimorph actuator.

2.2. Hot-leg/cold-leg actuator

These devices belong to the second category (ii) and are the most frequently used electrothermal in-plane actuators due to the simple one-mask fabrication process (figure 6) and because large deflection (up to 15 μm) and force ranges (up to 10–12 μN) can be achieved.

In the maximum tip displacement versus actuation power characteristic (figure 7) of the actuator with geometry listed in
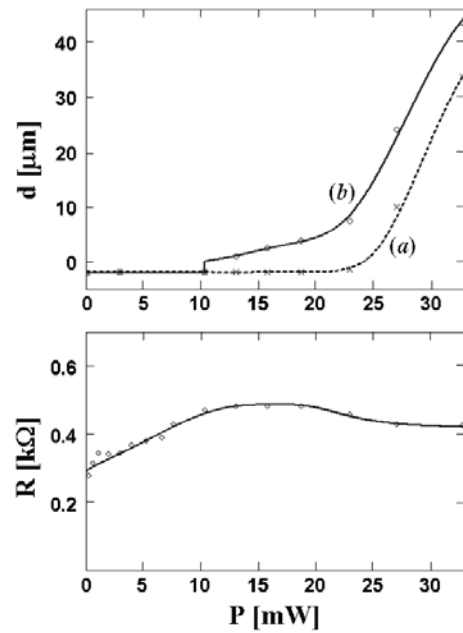
Figure 5. Maximum tip displacement versus electrical power and electrical resistance versus power characteristics of the trimorph actuator (under vacuum): (a) neutral position; (b) maximum tip deflection.

Figure 6. Sketch of hot-leg/cold-leg actuator (top-view).

Table 3. Geometrical characteristics—hot-leg/cold-leg actuator.

Geometrical characteristics	Dimensions (μm)
Hot legs	320×2
Cold leg + flexure	$275 \times 20 + 45 \times 2$
Connection of the legs at tip	5×2
Contact pads	115×110

table 3, the back-bending mode for high actuation powers that corresponds to the descending branch of the resistance versus power characteristic can be observed.

Two regions can be distinguished where this particular actuator does not change the neutral position for certain intervals of actuation powers: below 30 mW and above 60 mW. Although different authors use the 'back-bending' zone to assemble micromechanisms after fabrication [2], we have not succeeded in identifying measurements or input parameters that could definitely distinguish the back-bending regime from the region where failure occurs. Operating the actuators on the ascending branch of the resistance versus power characteristic ensures the reproducible actuation performance that we need for our micro-tribological studies.

2.3. Double-clamped parallel beams

This actuator belongs to the third (iii) category of electrothermal actuators and it consists of two double-clamped
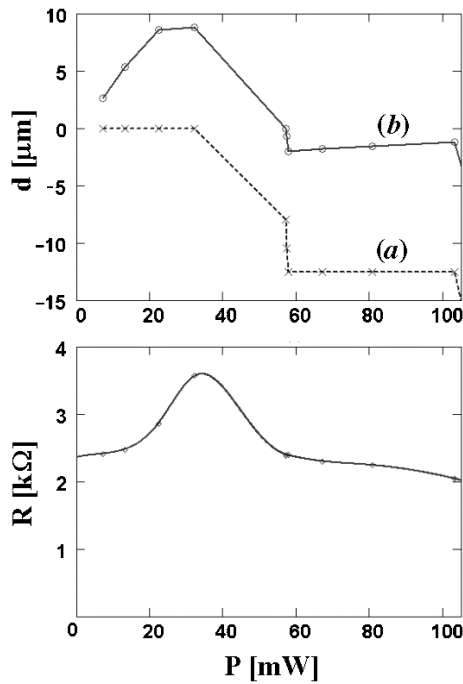
Figure 7. Maximum tip displacement versus electrical power and electrical resistance versus power of the hot-leg/cold-leg actuator (environmental conditions): (*a*) neutral position; (*b*) maximum tip deflection.
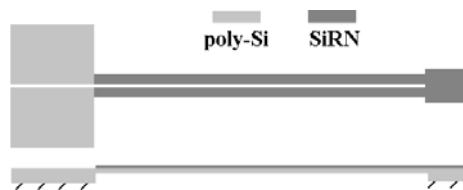
Figure 8. Sketch of the double-clamped parallel-beams: top-view (upper graph) and cross-view (lower graph).
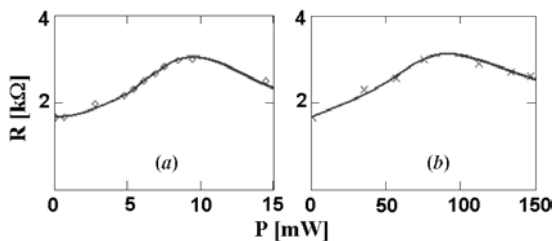
Figure 9. The resistance change versus actuation power for double-clamped parallel-beams: (*a*) under vacuum, (*b*) in ambient conditions.

beams of bimorph structure (poly-Si and SiRN—figure 8). The stress gradient through the structure determines the preferential buckling direction once the beams are resistively heated. The two 300 μm long and 4 μm wide beams separated by a 4 μm gap are clamped at both sides but electrically connected only at one end.

A comparison of the resistance versus power characteristics for tests performed in ambient conditions and under vacuum is presented in figure 9. The measurements suggest that the thermal power loss due to conduction through
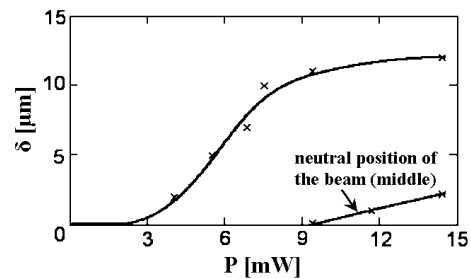
Figure 10. The maximum deflection and the change of the neutral position for double-clamped beam due to so-called 'plastic deformation' under vacuum.

air and primarily to the substrate is about 90% for actuation at the same performance, and in both cases the same phenomenon occurs. The maximum deflection of the middle of the beam measured in ambient conditions was a little bit larger ($\sim$1–2 μm) than in vacuum due to conduction through air, which changes the temperature distribution along the beams [19].

Even though the beam is double-clamped there is a change of the neutral position of the middle of the beam when it is actuated at high power (figure 10), which also coincides with the peak of the resistance versus power curve.

3. Discussions

Preliminary measurements with near-infrared camera (wavelength <1.1 μm) have been performed in order to estimate the temperature at which permanent deformation initiates. The camera was mounted on an optical microscope and images for different actuation power have been captured in ambient condition. The calibration of the temperature measurement was done on identical actuators (structure and materials) placed on a heater element that could be heated up to 1000 °C. It is extremely important to calibrate the measurement for the same material as the actuator consists of, since thermal radiation coefficients are both material and surface dependent. Due to 1.1 μm maximum wavelength of the camera the lowest detectable temperature was limited to about 450 °C for the double-clamped parallel beam. In figure 11 images grabbed with the near-infrared camera are presented. For symmetry consideration and sufficient optical magnification each picture shows half-length of a pair of actuated double-clamped beams. Figure 11(*a*) represents the actuator operated at 65 mW for which the estimated maximum temperature was 610 °C and the measured out-of-plane displacement of the middle of the beam 6 μm. The last measurement within the reversible actuation region was performed at 75 mW (figure 11(*b*)), which corresponds to a maximum temperature of 770 °C and gives 7 μm deflection. Taking into account the limited precision of the temperature measurement technique, we can estimate that the permanent deformation for this particular device initiates at local temperatures around 800 °C, clearly far below the intrinsic temperature of our highly doped poly-silicon.

The actuators have also been operated with AC square wave signals. The maximum frequency at which they could be actuated in ambient condition was limited to 17 Hz due to thermal inertia, but this value is design dependent. Operation
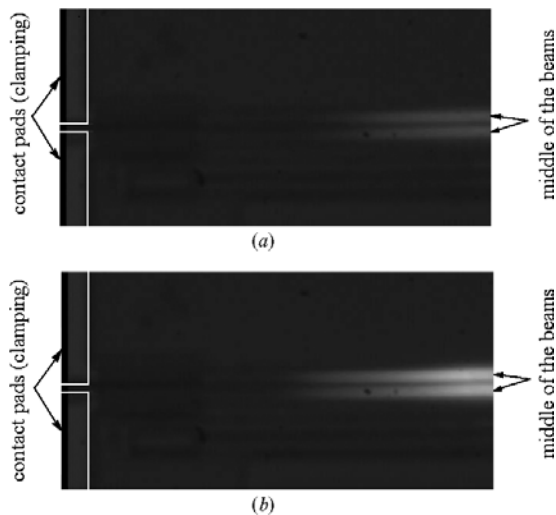
Figure 11. Temperature measurement on double-clamped beams with near-infrared camera (half-length of a pair of double-clamped beams for symmetry consideration): (*a*) actuator operated at 65 mW; (*b*) actuation at 75 mW. The contours of the contact pads are drawn for guidance of the eye.
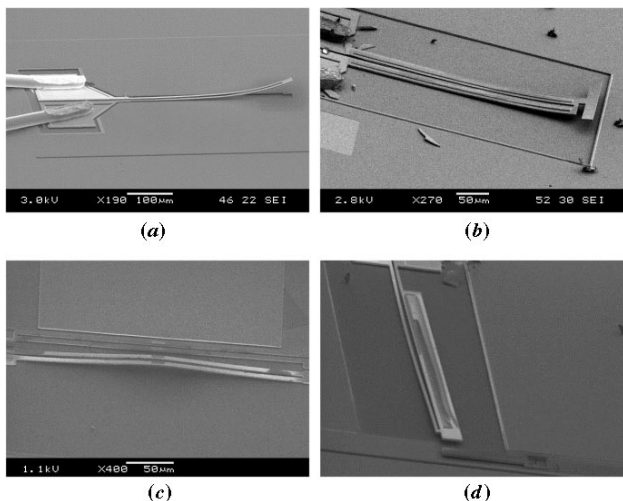
Figure 12. SEM photographs of actuated (*a*) bimorph actuator, (*b*) trimorph actuator, (*c*) double-clamped parallel-beams and (*d*) B-doped poly-Si hot-leg/trimorph cold-leg (tilted SEM table).

of the actuators in the reversible region for a few thousand cycles (several minutes) did not lead to irreversible behavior.

The SEM photographs of all tested actuators in the operating position are shown in figure 12.

4. Conclusions

It has been shown that the change of the neutral position of the B-doped poly-Si based electrothermal actuators coincides with operational powers at which the electrical resistance versus actuation power characteristic reaches a maximum. This can be used beneficially to distinguish the reversible and irreversible actuation zones no matter which is the working principle of these actuators and in which environment they are operated. Although this finding was experimentally observed

specifically for B-doped poly-Si actuators, we do expect that comparable behavior may be observed for other (poly-) crystalline semiconductor based actuators. Contrarily, other materials, e.g. metal-based actuators, will not show the same characteristics.

Due to fabrication process dependence of the properties of the materials this experimental method is appropriate to obtain the full capacity of the electrothermal actuators with reproducible performance. It is important to mention that one actuator from each specific design has to be characterized beyond the reversible limit before other identical actuators can be used at full performance. The method requires only a very simple measurement setup whereas other methods may be more complex. The discrimination of the reversible and irreversible actuation regions based on optical microscopy may require sophisticated setups, e.g. white-light interference microscopes for out-of-plane motions, because initially the permanent deformation is small. This may be hard to detect by simple optical/mechanical techniques like micrometers attached to a microscope (e.g. for out-of-plane motion).

For our devices the observed changes in resistance are attributed to structural change of the material since the doping levels are very high, thus the intrinsic temperature is much higher than the temperature at which the onset of structural changes are found.

References

[1] Reid J R, Bright V M and Butler J T 1998 Automated assembly of flip-up micromirrors *Sensors Actuators* A **66** 292–8
[2] Comtois H and Bright V M 1997 Applications for surface-micromachined polysilicon thermal actuators and arrays *Sensors Actuators* A **58** 19–25
[3] Pai M and Tien N C 2000 Low voltage electro-thermal vibromotor for silicon optical bench applications *Sensors Actuators* A **83** 237–43
[4] Conant R A and Muller R S 1998 Cyclic fatigue testing of surface-micromachined thermal actuators *MEMS, ASME, DSC*-vol 66 pp 273–7
[5] Maloney J M, Schreiber D S and DeVoe D L 2004 Large-force electrothermal linear micromotors *J. Micromech. Microeng.* **14** 226–34
[6] Kamins T 1998 *Polycrystalline Silicon for Integrated Circuits and Displays* (Dordrecht: Kluwer) chapter 5
[7] Pearson G L and Bardeen J 1949 Electrical properties of pure silicon and silicon alloys containing boron and phosphorus *Phys. Rev.* **75** 865–83
[8] Deladi S, Krijnen G and Elwenspoek M C 2003 FEM assisted design and simulation of novel electrothermal actuators *Proc. NanoTech'03* vol I, pp 400–3
[9] Deladi S, Krijnen G and Elwenspoek M C 2004 Parallel-beams/lever electrothermal out-of-plane actuator *Microsys. Technol.* at press
[10] Deladi S, Boer M J de, Krijnen G J M, Rosén D and Elwenspoek M C 2003 Innovative process development for a new micro-tribosensor using surface micromachining *J. Micromech. Microeng.* **13** S17–S22
[11] Sehr H, Evans A G R, Brunnschweiler A, Ensell G J and Niblock T E G 2001 Fabrication and test of thermal vertical

bimorph actuators for movement in the wafer plane
J. Micromech. Microeng. **11** 306–10

[12] Noworolski J M, Klaassen E H, Logan J and Petersen K E 1996
Process for in-plane and out-of-plane single-crystal-silicon
thermal micro-actuators *Sensors Actuators* A **55** 65–9

[13] Chen W C, Hsieh J and Fang W 2002 A novel single-layer
bi-directional out-of-plane electro-thermal microactuator
IEEE MEMS 2002, pp 693–7

[14] Que L, Park J S and Gianchandani Y B 2001 Bent-beam
electrothermal actuators: Part I. single beam and cascaded
devices *J. Microelectromech. Syst.* **10** 247–62

[15] Kolesar E S, Ko S Y, Howard J T, Allen P B, Wilken J M,
Boydston N C, Ruff M D and Wilks R J 2000 In-plane tip
deflection and force achieved with asymmetrical polysilicon

[16] Cragun R and Howell L L 1998 A constrained thermal
expansion micro-actuator *MEMS, ASME*, *DSC*-vol 66
pp 365–71

[17] Sinclair M 2002 A high frequency resonant scanner using
thermal actuation *IEEE MEMS 2002*, pp 698–701

[18] Chiao M and Liwei L 1997 Microactuators based on
electrothermal expansion of clamped-clamped beams
MEMS, ASME, *DSC*-vol 62/*HTD*-vol 354 pp 75–80

[19] Baar J J van, Wiegerink R J, Lammerink T S J, Krijnen G J M
and Elwenspoek M C 2001 Micromachined structures for
thermal measurements of fluid and flow parameters
J. Micromech. Microeng. **11** 311–8

electrothermal microactuators *Thin Solid Films* **377–378**
719–26